

Measurement of dynamic deformation using a superimposed grating

B. Barrientos and M. Cywiak
*Centro de Investigaciones en Óptica,
37 150 León Gto. Méx.*

W.K. Lee and P. Bryanston-Cross
*Optical Engineering Group, University of Warwick,
CV4 7AL UK.*

Recibido el 26 de agosto de 2002; aceptado el 27 de mayo de 2003

Mechanical devices are normally used under conditions of dynamic motion. Due to resonance effects, this condition produces undesired modes of vibration, which are necessary to be measured for satisfactory design. This paper describes a method to measure the temporal development of the vibrational modes in mechanical objects subjected to external vibration, by a double exposure fringe technique. A grating placed directly on the object under study serves as a carrier frequency, which enables automatic phase calculation. This grating, which is imaged by a commercial digital camera, used in conjunction with a spatial carrier fringe method for phase evaluation, allows determining the vibration deformation. This technique is suitable for the analysis of rapid transient events since no movable parts are required in the system. The obtained range of deformation by the proposed method goes from a few tenths of micrometers to millimetres.

Keywords: Dynamic deformation; fringe projection; spatial carrier fringe method; double exposure method.

Los dispositivos mecánicos se utilizan normalmente bajo condiciones de movimiento. Esto puede producir efectos de resonancia tal que originen modos de vibración. Estos modos de vibración deben medirse para asegurar un diseño satisfactorio. En este artículo se describe un método para medir el desarrollo temporal de modos de vibración en objetos mecánicos, los cuales son sometidos a vibración externa mediante una técnica de franjas de doble exposición. Una rejilla colocada directamente sobre el objeto actúa como frecuencia portadora permitiendo el cálculo automático de la fase óptica. Tal rejilla, cuya imagen es capturada mediante una cámara digital comercial, usada en conjunto con un método espacial de franjas portadoras para evaluación de la fase, permite la determinación de la deformación por vibración. La técnica es propuesta para el análisis de eventos transitorios rápidos, ya que el sistema no requiere de partes móviles. El intervalo de aplicación de medición de deformación va desde decenas de micrómetros hasta el orden de milímetros.

Descriptores: Deformación dinámica; proyección de franjas; método de franjas de portadora espacial; método de doble exposición.

PACS: 4630Rc.

1. Introduction

Fringe projection has been applied successfully in problems related with the analysis of shape of biological specimens [1] and mechanical parts [1-7]. In the fringe projection technique [3], an image of fringes is projected onto the object under investigation and a photographic image is made of the illuminated surface. Generally, the projected fringes correspond either to a grating or to the superposition of two coherent beams. In this report, a print of a grating is directly superimposed on the object under study in order to avoid any projection optics and have a simple measuring system. Observation is done at a certain angle with respect to the overall normal of the object. Thus, the observed fringes depend on both the topography of the specimen and the observation direction.

Fringe projection techniques are widely used because of their insensitivity to external noise sources and their feasibility to be applied to large spatial regions at once in a non-contact way. The use of white light implies simple arrangements and the possibility of applying this technique in industrial environments. Furthermore, when gratings are placed directly on the specimens the range of object sizes that can be tested is large.

In the projection method, the projected grating leads naturally to the use of fringe carrier methods for optical phase assessment [4]. Other phase evaluation methods have been previously applied in fringe projection, namely temporal phase unwrapping [5], phase stepping [3], spatial synchronous detection [6], and zero-crossing detection [2].

In the present work, we propose the use of a fringe carrier method in conjunction with double-exposure [8] for the measurement of out-of-plane deformation. The object is imaged at two different deformation states and the resulting images are compared. The optical phase due to deformation is calculated using the difference of phase method [9-10]. In this method, the optical phase is calculated at an arbitrary reference state using the Fourier carrier fringe method [4] for instance and a second phase map is similarly calculated for a second image in another arbitrary deformation state. The difference of the resulting phase maps defines the relative deformation between both states. In this work, no unwrapping of the resulting phase is necessary since the relative deformation is of the order of a fraction of a grating period.

The range of measurement of our proposed method goes from a few tenths of micrometers to millimetres. Thus, such a measurement range complements that obtained with inter-

ferometric and speckle methods, where deformations up to a few micrometers are observed [11].

2. Experimental set-up and mathematical support

Figure 1 shows the experimental set-up of the proposed method. A white light Xenon flash lamp is used to illuminate the object, which is imaged into a commercial digital camera of 1368×1712 pixels. A simple flat object was chosen for demonstrating purposes. The object, a $30 \times 33 \times 0.2$ cm aluminium plate, is driven by a mechanical vibrator (MV) attached to its surface. The working frequencies of the MV are related to the natural vibration modes of the aluminium plate. For illustrative purposes, we have selected a range from 100 Hz to 1100 Hz for this experiment; this range excites

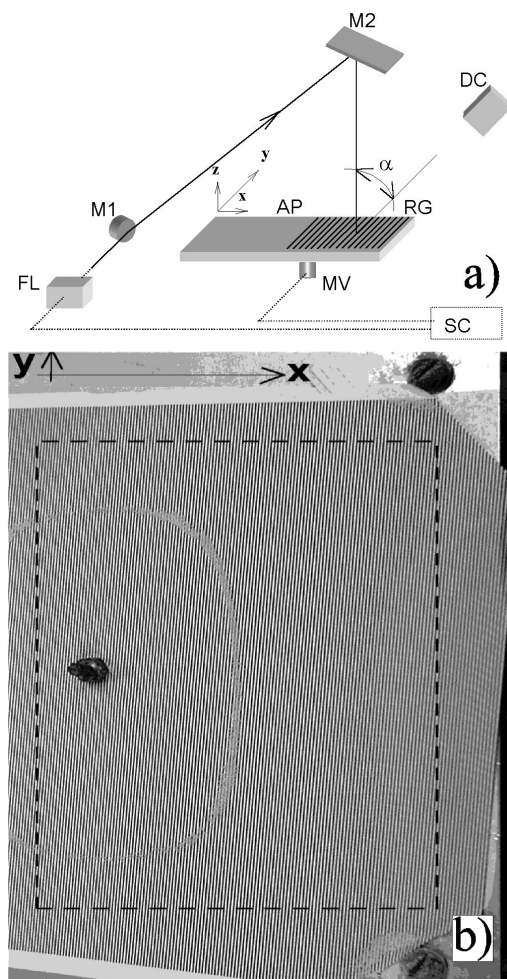


FIGURE 1. a) Schematic arrangement of the proposed system. AP: Aluminium plate; M1 and M2: Mirrors; FL: Xenon flash lamp; MV: Mechanical vibrator; RG: Ruling grating; DC: Digital camera; SC: Synchronisation circuit. b) Photograph of the object under test, while vibrating at 185 Hz. The region in the dashed rectangle corresponds to the observation region (right side of the object). The excited natural vibration mode is made visible by scattering small particles on the object surface.

approximately the first 10 low frequency vibrational modes. The plate is clamped at its four corners.

As described above, our method uses a grating to generate modulation of the signal under detection. For this purpose, a hard copy of a binary grating was fastened to the plate surface. The period of the grating is 0.93 mm. In section three, we describe how this period is selected. A 50% duty cycle is selected to resemble a sinusoidal profile, which simplifies the mathematical approach, although it does not affect the overall result.

Due to the symmetry of both the object under study and of the loading conditions, we find similar results for the left and right halves of the surface under test. We present results for the right half of the object. This observation region is indicated by a dashed rectangle of 20×25 cm in Fig. 1b.

The distance between the mid point of the observation region of the surface under test and the digital camera is 57.0 cm (distance between point B and digital camera in Fig. 2), and the mean angle between the optical axis of the camera and the normal to the plate, α , is 30.8° . The vibrator is located at the centre of the aluminium plate. The grating is imaged onto the camera in a horizontal direction with respect to the sides of the camera sensor. As shown in Fig. 1b, in this geometry of the setup, perspective effects cannot be avoided. However, in the double exposure method the error term arising from perspective is cancelled as long as the deformation between consecutive acquisitions is not greater than a few grating periods. This is shown below.

The camera was set at an F-number of 8 and exposure time of 0.1 s. In order to avoid multiple exposures on the same frame, since the exposure time was hold constant, the flash lamp was fed at a multiple of the driving frequency of

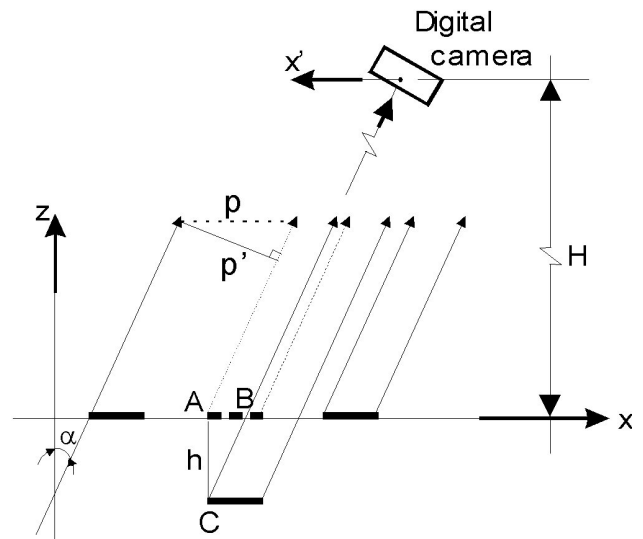


FIGURE 2. Geometry used in the calculation of the out-of-plane deformation, $h(x, y)$. As the object is deformed from point A to C, the horizontal position of the grating changes from x_A to $x_B = x_A + h \tan \alpha$ as seen by digital camera, where x_A is the x-reference position of point A. Here H stands for the perpendicular distance from the digital camera to the plane of the object.

the vibrator. The synchronisation between the camera, flash lamp and vibrator was implemented through the synchronisation scheme depicted in Fig. 3.

A sinusoidal wave generator (SWG) is used to generate the master signal of the synchronisation scheme shown in Fig. 3a. This signal drives the external triggers of the variable-delay pulse generator and that of a mechanical vibrator (MV). This latter signal is input into channel A for monitoring purposes. The pulse generator in turn drives the flash lamp. The pulse generator can vary the time between a reference position of the sinusoidal wave, which drives MV, and the illumination of the object. This latter signal, which drives the flash lamp, is input into channel B of the oscilloscope, as is shown in Fig. 3b. Thus, both driving signals are detected simultaneously on the oscilloscope. This allows us to vary the position of the illumination pulse, t_d , in a precise way with respect to the deforming movement.

A typical value for the deformation period is 5 ms. This deformation cycle is scanned by varying the delay time, t_d . As it is shown in section three, the illumination pulse width can be selected as to freeze the object motion in time. This means, that the resulting images contain all the necessary data about the object for the calculation of the deformation. In this case, since the frequency of the grating attached to the surface acts as the carrier frequency, we have that the gray

level of an image as detected by the digitizing camera can be represented as [12]

$$I_{\text{und}}(x, y) = a(x, y) + b(x, y) \cos(\varphi(x) + \theta(x, y)), \quad (1)$$

for a reference state, where $\varphi(x)$ contains the phase due to the carrier term and that due to the height distribution of the object, $\theta(x, y)$ represents the phase contribution from both perspective and variation of the optical magnification of the camera, and $a(x, y)$ and $b(x, y)$ are the coefficients of bias and contrast of the fringes, respectively. In our case, the perspective term corresponds to a contribution to the phase term mainly in the x-direction. In Eq. (1) only the first frequency component of the grating has been taken into account.

Any deviation of the fringe distribution represented by Eq. (1) is related to a change of the object shape. This can be expressed as

$$I_{\text{def}}(x, y) = a(x, y) + b(x, y) \cos(\varphi(x) + \theta(x, y) + \phi(x, y)), \quad (2)$$

where it has been assumed that the deformation represented by $\phi(x, y)$ is small so as not to change significantly the bias and the modulation terms. If the deformation is of the order of a few grating periods, the perspective-magnification contribution term $\theta(x, y)$ remains practically unchanged, as it is shown below.

When using the Fourier extracting phase method the intensity patterns are mapped onto the Fourier domain. In this domain, they are band-pass filtered and then returned to the spatial domain. Then, the arguments (phases) of the sinusoidal terms in Eqs. (1) and (2) are computed [4]. The filtering process in the Fourier domain removes low-frequency terms, such as the bias term, and frequency components greater than the sum of the carrier frequency and the highest deformation frequency component, e.g. spurious noise. Higher frequency components of the grating are filtered out as well.

Once the phase arguments are calculated for any two states, their phase difference corresponds to their relative deformation, $\phi = [\varphi + \theta + \phi] - [\varphi + \theta]$. As it is seen, after taking the difference of the phase terms, the perspective contribution $\theta(x, y)$ is fully compensated.

From Fig. 2, considering ΔABC , it can be shown that the relationship between the phase term stemming from deformation, $\phi(x, y)$, and the actual out-of-plane deformation, $h(x, y)$, can be expressed by [7,12]

$$h(x, y) = \frac{\phi(x, y)}{2\pi} \frac{p}{\tan \alpha}, \quad (3)$$

where p is the grating period and α the mean angle between the observation direction and the normal of the plate. In Eq. (3) it has been assumed that the observation distance is much larger than the dimensions of the observation region. As it can be seen from Eq. (3), the range of deformation of the method can be varied by properly selecting the grating period and the observation angle.

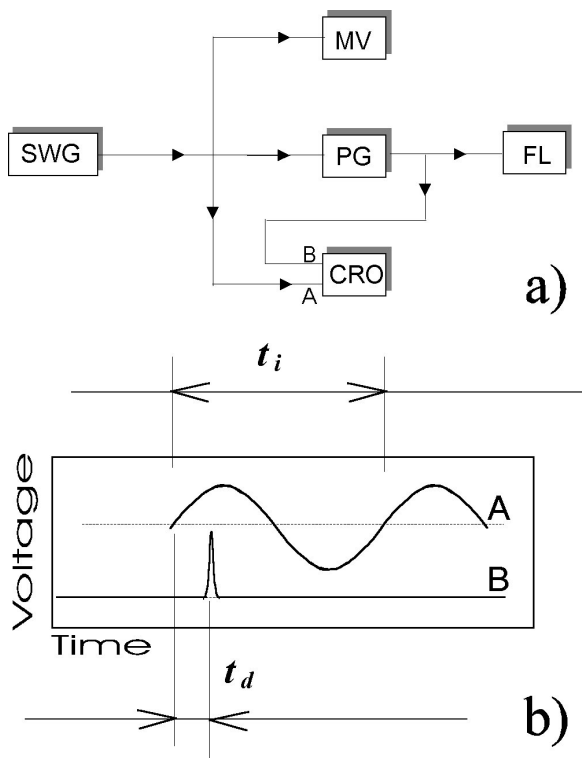


FIGURE 3. a) Synchronization circuit. SWG: Sinusoidal wave generator; PG: Variable-delay pulse generator; MV: Mechanical vibrator; CRO: Oscilloscope; FL: Xenon flashlamp. b) Monitoring of signals driving MV and FL respectively. Here t_i is the period of the excitation signal to MV.

To estimate the maximum limit of deformation that can be measured with our method, we first obtain a relation of the apparent grating period (p') as seen by the camera, and the distance between the digital camera and the object plane along the z -direction (H). From the geometry depicted in Fig. 2, we obtain,

$$p' = p \frac{H}{\sqrt{H^2 + (x')^2}}, \quad (4)$$

where x' is the x -position with respect to the digital camera.

Secondly, we differentiate Eq. (4) to estimate the change of the apparent grating period as a function of the variation in H , *i.e.*,

$$\Delta p' = p \left[\frac{1}{\sqrt{H^2 + (x')^2}} - \frac{H^2}{(H^2 + (x')^2)^{3/2}} \right] \Delta H, \quad (5)$$

Finally, we compute the maximum value for $|\Delta H|$, which is equivalent to the maximum out-of-plane deformation that can be measured.

At this point, it is convenient to notice that an expression identical to Eq. (5) can be found for the variation of the period as a function of the variation of the magnification of the digital camera. In this latter case, it is assumed that the image distance of the digital camera is constant.

According to Eq. (5) and taking into account the last two mentioned sources of variation of the grating period, we find that the maximum value for $|\Delta H|$ is 11 mm in our experimental setup. To obtain this value, we have used the following experimental conditions: maximum value of x' 37.5 cm, maximum $\Delta p'/p = 1/80$ and $H = 50$ cm. Notice that the latter values are chosen for the worst experimental conditions and that the allowed variation in the grating period is of the order of the fluctuation due to noise, as described in the next section.

In the reported measurements, the obtained out-of-plane deformation is well below this limit. Thus, the variation of the period because of the difference in perspective and magnification for two deformation states can be neglected.

When the relative deformation is greater than the allowed ΔH , the phase term arising from perspective and variation of magnification is no longer fully compensated between two deformation states. In order to reduce this effect, it is possible to calculate the deformation between two closer deformation states and use an updated reference [13]. This would enable us to increase the range of deformation of the method.

3. Results and discussion

For the present results, the sensitivity of the set-up is 1.56 mm/fringe (according to Eq. (3) with $\alpha = 30.8^\circ$ and grating period of 0.93 mm). When selecting the grating period, care is taken to maintain a well-resolved image of the grating and fulfil within the Nyquist sampling frequency.

It is important to notice that while moving the object sinusoidally, the illumination time was much shorter than the

period of the vibration t_i ($t/t_i < 0.2$, where t is the illumination pulse width); this ensures that the resulting change in phase is entirely associated with the shape of the object at any vibrating state according to Eqs. (1) and (2) [14].

In order to obtain the deformation at a specific point in the vibrating cycle of the object relative to a reference position, we first calculate a reference phase by means of Eq. (1). Next, the optical phase due to deformation is calculated by means of Eq. (2). The two phases so obtained are subtracted and the deformation is obtained through Eq. (3). In the reported measurements, no unwrapping of the resulting phase is necessary since the relative deformation is less than a grating period. In the case of larger deformations (*e.g.* a few grating periods), any of the available unwrapping algorithms can be applied to the resulting phase map in order to calculate the out-of-plane deformation.

A typical image representing Eq. (1) or (2) is shown in Fig. 4. In this figure, we point out that the presence of the screw, which is needed to attach the mechanical vibrator to the aluminium plate, avoids that zone to be analysed because of the lack of modulation. Thus, a noise peak in the deformation results may appear in that region, as in Fig. 6a. In the rest of the results, the deformation values for this zone were computed by interpolation of the neighbouring points.

Next, we present three sets of measurements of the aluminium plate, in which the resonance frequency is different.

Figure 5 shows the resulting out-of-plane displacement at different temporal points (temporal phases, t_d) through the vibration cycle of the aluminium plate (Figs. 5a-5b). They correspond to the first resonance mode at a frequency of 107 Hz. Fig.5c shows the deformation along a line passing through the centre of the latter images in the x -direction.



FIGURE 4. A typical image used in the calculation of the optical phase.

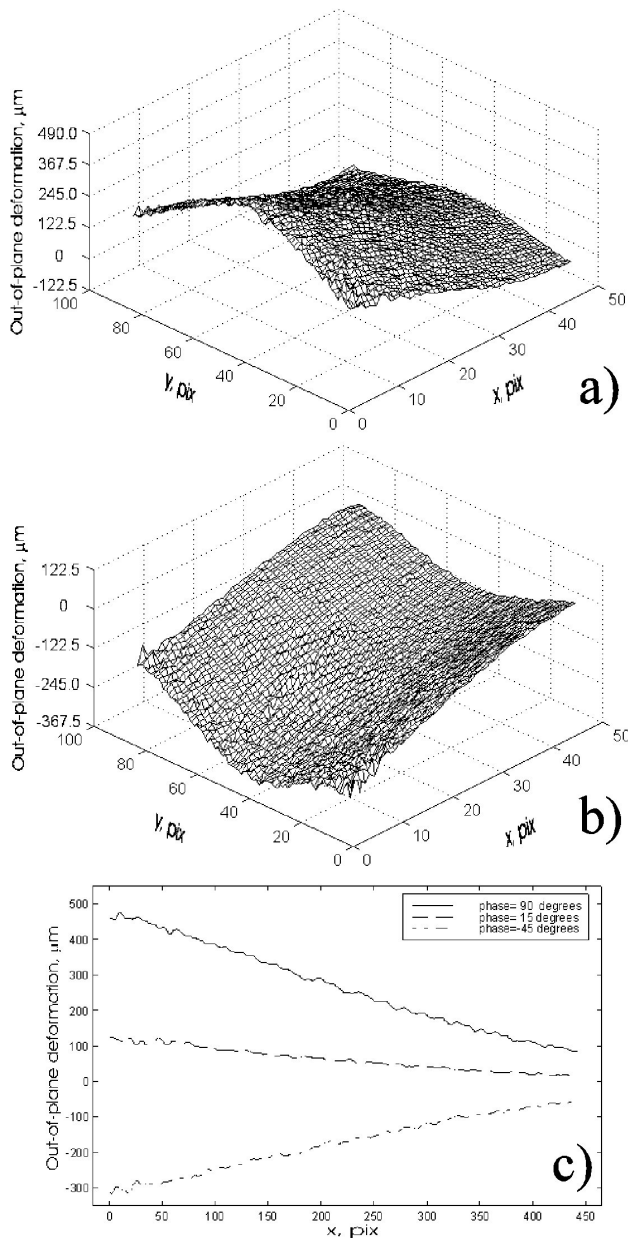


FIGURE 5. Out-of-plane deformation at different phase points of the vibration cycle of the first oscillation mode at 107 Hz; the vertical axis corresponds to the z-direction. a) $t_d=90^\circ$, b) $t_d=-45^\circ$, and c) Displacement along a central line (x-direction) of the observed region at different temporal points in the vibration cycle. In a) and b) the axes were sampled every 20 pix while in c) every 2 pix. A region of 450 pix on the left side of the figures (in the x-direction) was neglected.

These results agree well qualitatively with the nodal patterns observed when small particles are scattered over the aluminium plate, as it is shown in Fig. 1b.

The resulting out-of-plane deformation of the second vibration mode at 185 Hz is shown in Fig. 6. We can notice a decrease in the magnitude of the displacement and the existence of a piston-like displacement of $-25 \mu\text{m}$ (Fig. 6c). The piston-like displacement is associated with the reference displacement that the plate undergoes between consecutive sets

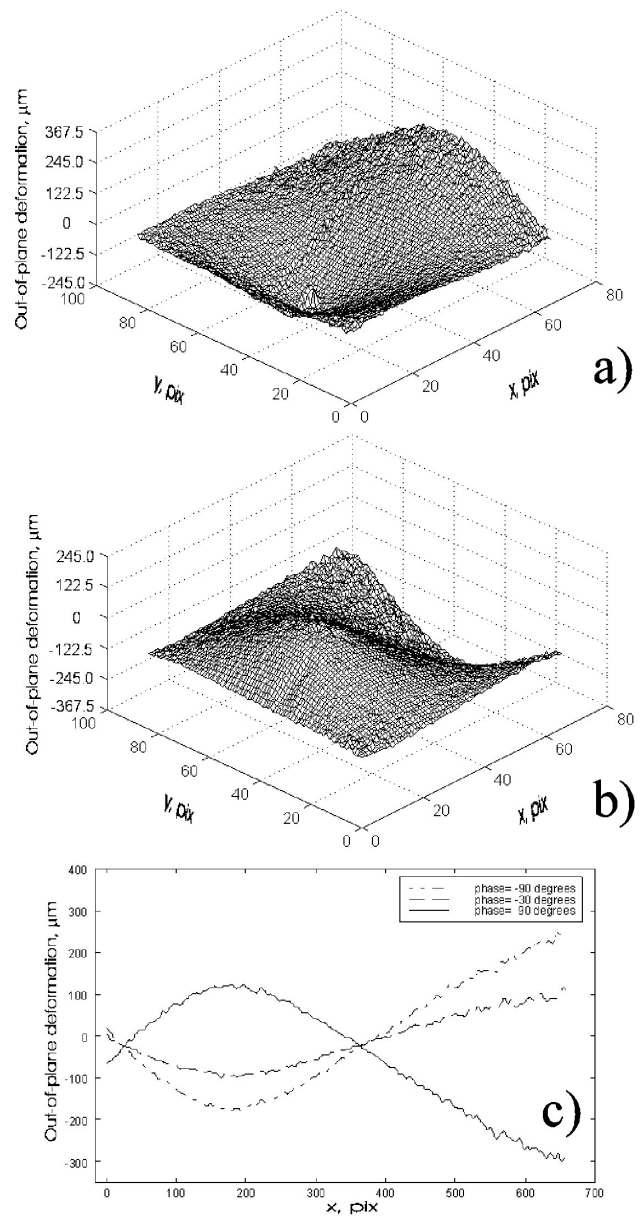


FIGURE 6. Out-of-plane deformation at different phase points of the vibration cycle at 185 Hz. a) $t_d = -90^\circ$, b) $t_d = 90^\circ$, and c) Displacement of the central line (x-direction) of the observed region at different temporal points in the vibration cycle. In a) and b) the axes were sampled every 20 pix while in c) every 2 pix.

of measurements when the mechanical vibrator is not initialised. This piston-like displacement is then contained in the reference state, and when comparing a deformation state with the reference state it appears as a bias deformation. If we take a vibrating state as the reference state, this bias term is cancelled.

To see the effect of noise, two static images are taken within an interval of some minutes and the difference in the deformations is computed. The fluctuation due to noise is less than $\pm 2\pi / 80$ rad rms (or equivalently $\pm p/80$).

In the limit of the sensitivity of the set-up, the precision of the measurements is low. However, they can still draw some

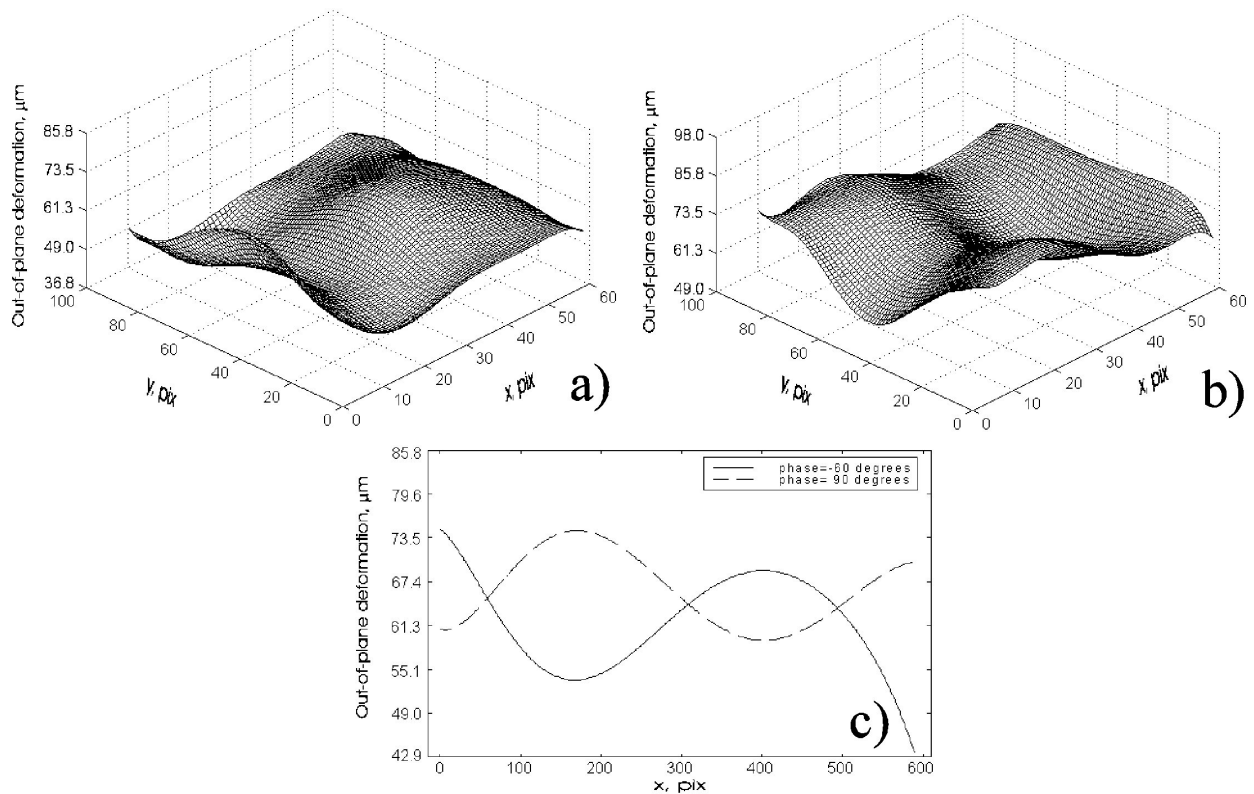


FIGURE 7. Out-of-plane deformation at different phase points of the vibrating cycle at 1025 Hz. a) $t_d = -60^\circ$, b) $t_d = 90^\circ$, and c) Displacement of the central line of the observed region at $t_d = -60^\circ, 90^\circ$. In a) and b) the axes were sampled every 20 pix while in c) every 2 pix. A region of 160 pix on the left side of the figures (in the x-direction) was neglected.

information on the deformation by performing a polynomial fit to the deformation data as is shown in Fig. 7. In this case, the resulting vibration at 1025 Hz has a piston term of about $64 \mu\text{m}$.

The depth of field of the camera defines the maximum size of the object that can be imaged before the image becomes blurred at some regions. As the size of the object increases the depth of field must be increased by reducing the recording system aperture. This in turn decreases the resolving power of the camera and therefore the measuring system becomes less sensitive since the frequency of the grating is limited by the Nyquist limit of the camera.

4. Conclusions

We have described a method to measure the temporal development of the vibrational modes in mechanical objects subjected to external vibration by a double exposure fringe pro-

jection technique. To illustrate how our method works, an aluminium plate was clamped at its four corners and subjected to external vibration via a mechanical vibrator placed at its centre. This produced vibrational modes in the plate, which were measured as they developed in time. To do this, a hard copy of a grating was attached on the plate and a comparison of the optical phase of two states of the plate, via Fourier carrier fringe techniques, was done. The attached grating acts naturally as the carrier frequency, avoiding the use of movable or switching devices, as necessary in phase stepping. Furthermore, since our method does not require the projection of fringes, the system becomes experimentally simple.

We have shown analytically that aberrations in the system are cancelled, as long as the relative deformation is not greater than a few grating periods. This implies that high accuracy measurements are achieved without the need of calibration with a reference surface.

1. R. Windecker and H. J. Tiziani, "Topometry of technical and biological objects by fringe projection," *App. Opt.* **34** (1995) 3644.
2. G. Indebetouw, "Profile measurement using projection of running fringes," *App. Opt.* **17** (1978) 2930.
3. E. Srinivasan, H. C. Liu and M. Alioua, "Automated phase-measuring profilometry of 3D diffuse objects," *App. Opt.* **23** (1984) 3105.
4. M. Takeda and K. Mutoh, "Fourier transform profilometry for

- the automatic measurement of 3-D object shapes,” *App. Opt.*, **22** (1983) 3977.
5. H. O. Saldner and J. M. Huntley, “Temporal phase unwrapping: application to surface profiling of discontinuous objects,” *App. Opt.* **36** (1997) 2770.
 6. S. Tang and Y. Y. Hung, “Fast profilometer for the automatic measurement of 3-D object shapes,” *App. Opt.* **29** (1990) 3012.
 7. B. Dessus and M. Leblanc, “The ‘fringe method’ and its application to the measurement of deformation, vibrations, contour lines and differences of onjects,” *Opto-electronics* **5** (1973) 369.
 8. E. Archbold and A. E. Ennos, “Displacement measurement from double-exposure laser photographs,” *Opt. Acta* **19** (1972) 253.
 9. D.W. Robinson and D.C. Williams, “Digital phase stepping speckle interferometry,” *Opt. Comm.* **57** (1985) 26.
 10. A.J. Moore, J.R. Tyrer and F. Mendoza S, “Phase extraction from electronic speckle interferometry addition fringes,” *App. Opt.* **33** (1994) 7312.
 11. T. Kreis, “Holographic interferometry: Principles and Methods,” Akademie Verlag, Berlin 1996.
 12. K. Creath and J.C. Wyant, “Comparison of interferometric contouring techniques,” *SPIE* **954** (1988) 174.
 13. S. Nakadate and H. Saito, “Fringe scanning speckle-pattern interferometry,” *App. Opt.* **24** (1985) 2172.
 14. A. J. Moore, D. P. Hand, J. S. Barton, and J. D. C. Jones, “Transient deformation measurement with electronic speckle pattern interferometry and a high-speed camera,” *App. Opt.* **38** (1999) 1159.